Design and fabrication of bimodal meso-mesoporous WO_3 thin films and their electrochromic properties

Wei Wang, Yongxin Pang, Simon N. B. Hodgson*
School of Science and Engineering, Teesside University, Midddlesbrough, Tees Valley, TS1 3BA,UK

Graphic content entry:

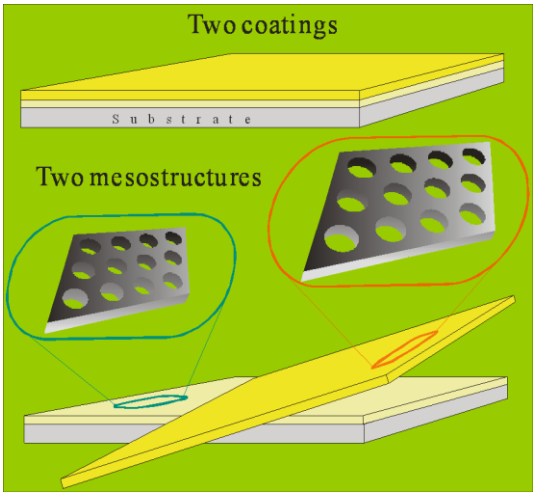

A novel, facile and reliable two-step coating process has been developed to produce bimodal meso-mesoporous (BMM) tungsten oxide films (TOFs) by taking advantage of the thermal-dependence of tungstic acid/Brij56 derived sol-gel TOFs selectively sensitised by chemical modification to the inorganic tungsten oxide species. Importantly, such BMM structures are able to be delicately tailored by simple heat-treatment at different temperatures.

Summary

Based on a novel, facile and reliable two-step coating process, tungsten oxide films (TOFs) with bimodal mesoporous-mesoporous structure (BMM) were designed and realised in terms of a bilayered mesostructural configuration. The key step for successful fabrication of these BMM TOFs is the selective thermal sensitisation of the tungstic

* Corresponding author: Prof. Simon Hodgson, School of Science and Engineering, University of Teesside, UK. Tel: +44 (0)1642 384314, Fax: +44(0)1642 342401, Email: s.n.hodgson@tees.ac.uk

acid/Brij 56 derived sol-gel TOFs in by different chemical modification to the inorganic tungsten oxide species. Moreover, one striking advantage of this process lies in that it also allows delicate tailoring of the resulting BMM structures by simple heat-treatment at different temperatures. According to the initial test results on the electrochromic properties, the obtained BMM TOFs demonstrate superior performance over their monomodal counterparts.

1. Introduction

Since the discovery of a new family of mesoporous materials (M41S), featuring large surface area, high pore volume and ordered mesopores,[1] the fabrication of transition metal oxides-based mesoporous materials has attracted significant attention in pursuit of combining their diverse properties (e.g. catalytic, optical, electronic, magnetic, etc) with the features of mesoporous materials.[2]

In order to fulfil the demand on high surface area, specific pore size(s) or pore channel arrangements, increasing attention has been paid to tailor the pore systems of such kinds of materials. Some works were focused on one of the exciting areas, namely bimodal meso-mesoporous (BMM) materials. Currently, several methods have managed to synthesise BMM materials, e.g. utilising mixed surfactants,[3] gel phase separation process,[4] organic/inorganic compounds as additives,[5] two-step assembly process,[6] or post treatment with ammonia.[7] Such methods were predominantly designed and tested for silica or silica-based materials,[3a, 4, 5a-d, 6,7] with very limited approaches reported to date for the synthesis of BMM transition metal oxides.[3b,5e] This may arise from the fact that there are inherent difficulties on account of the facile crystallization of most of these oxides, which tends to cause structural collapse, during the formation of mesostructures and removal of the organic templates.[8] Hence, an innovative synthesis strategy is necessary to be explored to suit the transition metal oxide systems in order to achieve the desired BMM structures.

Mesoporous tungsten oxide with BMM structures, irrespective of form as powders or films, has not been reported yet. Indeed, tungsten oxide films (TOFs) have received substantial attention for smart windows applications due to its transparency and good reversibility in colour change when external electrical field is applied.[9] Mesoporous tungsten oxide films also showed improved colouration efficiency and colour–bleach kinetics.[10] Recently, we reported one simple and cheap surfactant templated sol-gel method to synthesise mesoporous TOFs,[11] following an evaporation-induced self-assembly (EISA) procedure.[12] In that work, thermally stable mesostructures were prepared from tungstic acid under systematically optimised synthesis conditions. This work further extends this novel approach to the fabrication of BMM structured TOFs.

Instead of developing BMM structured metal oxides in a single step as usually

performed,[3-7] it is also possible to sequentially pile up two coating films with different mesoscopic porosities to generate BMM structures in one bilayered film. In the extensively studied surfactant templating synthesis,[1-3] inorganic 'building materials' assemble around supramolecular surfactant structures, resulting in the formation of the desired mesostructures. Therefore, the size of supramolecular surfactant structure dictates to a large extent the pore sizes in the resultant mesoporous materials.[1b] Not surprisingly, bi- or multi-stacks of sol-gel films templated by surfactant molecules of different size can yield bi- or multi-modal mesoporous architectures.[13] Even for a single-surfactant templating system, the concentration of the surfactant, which has been demonstrated to have great influence on the mesostructures,[14] can be utilised to design bi- or multi-modal the mesostructures [15]. However, in this work, a novel approach is investigated to demonstrate if, rather than focusing on the tailoring of the templating behaviour of surfactants, is it possible to produce BMM structures by tailoring the inorganic 'building materials'?

In this work we propose and report a novel synthesis process leading to BMM structures of TOFs based on such an approach involving a two-step coating process followed by thermal treatments to induce the required structure, in combination with chemical modification to the peroxotungstic acid (PTA) species to impart differential thermal sensitivity. In this process, two sols used in the two sequentially coating steps have the same formulation, except that one is chemically modified to endow the PTA species with greater thermal dependence. The BMM TOFs fabricated by this method thus produce BMM structures which are *selectively tuneable* by heat treatment. The electrochromic properties of the resulting BMM structured TOFs are also investigated to assess their potential as electrochromic materials.

2. Results and discussion

It has been reported in our previous work that for the non-ionic surfactant templated PTA films, one of the main characteristics of the obtained mesostructures was the great flexibility of mesoframeworks, evidenced by the substantial 2θ shift in low-angle XRD peak positions upon heat-treatment.[11] The flexibility of the mesostructures is further testified by low-angle XRD results for the TOFs with a single coating, as shown in Fig. 1(a). The low-angle peaks in XRD patterns for PTA/Brij 56 hybrid films shift to higher angle with increasing heat treatment time and temperatures. Detailed changes in 2θ values and d-spacings with heat treatment conditions were listed in Table 1. For instance, heating at 170 ºC for 1 h led to an increment in 2θ value from 1.5º to 2.3º, with calculated d-spacings decreased from 5.9 nm to 3.8 nm on account of structural contraction. Similarly, prolonged heating up to 2 hours at 170 ºC resulted in further decrease in d-spacing from 3.8 nm to 3.5 nm. Importantly, after heating at 400 ^{o}C for 1 h (Fig. 1(a), curve 6), the low-angle XRD peak (2θ≈ 3.7^{o}, Table 1) is still observable, indicating the retention of mesostructures, though degraded to some extent evidenced by the broadening

of the FWHH from about 0.08° for as-dried TOFs to 0.33°. The single strong peak in each XRD pattern indicates a preferred orientation of the mesopores. Additionally, the shape of the diffraction peaks shown in these XRD patterns were consistent and did not change along with the heat treatments, suggesting no detectable changes in mesopore arrangement apart from structural contractions.

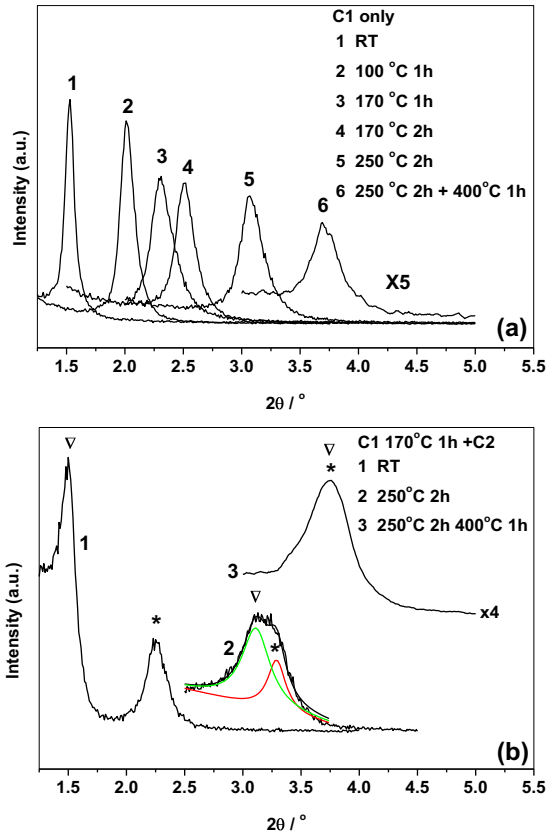

Fig. 1 XRD patterns of (a) C1 TOFs in the case of single coating ('x5' near curve 6 indicates that the intensity is magnified by a factor of 5, with the same notation applicable to other XRD patterns), (b) bimodal (C1+C2) TOFs heated at different temperatures. Inverted triangle represents the low-angle peak from C2 and asterisk the peak from C1. The de-convolution was carried out using Lorentzian peaks.

Fig. 2 shows the TEM images for the PTA/Brij56 hybrids films, heated at temperatures ranging from 100 °C to 400 °C, which provide direct evidences of the mesostructures. It can be seen from Fig. 2(a) that, after drying at 100 °C, mesostructures with hexagonal-like mesopore arrangement are present with mesopores (still occupied by organic template in this stage) of about 3 nm. Mesopores with pore size of about 2nm can also be seen from TOFs heated at 400 °C for 2 h (Fig. 2(c)). The ordering of mesopores deteriorated with the increased heating temperature, as can be seen from Fig. 2a to 2c. It is important to note that the TEM specimens are in the form of thin flakes from scratched TOF films and therefore, the TEM images show the structures observed in a direction

perpendicular to the original film surface. This means that, irrespective of heat-treatment conditions, the open pores/channels are accessible from the film surface. In electrochromism, the importance of these open-pore channels will be reflected in the easy cation diffusion.

Table 1 Textual parameters as a function of heat treatment conditions for a single coating TOF.

Heat treatment	As dried	100 °C/1h	170 °C/1h	170 °C/2h	250 °C/2h	250 °C/2h +400 °C/1h
2θ (º)	1.50	2.00	2.31	2.50	3.06	3.71
d_{110} (nm)	5.89	4.42	3.82	3.53	2.88	2.38
a	8.32	6.24	5.41	5.00	4.08	3.37

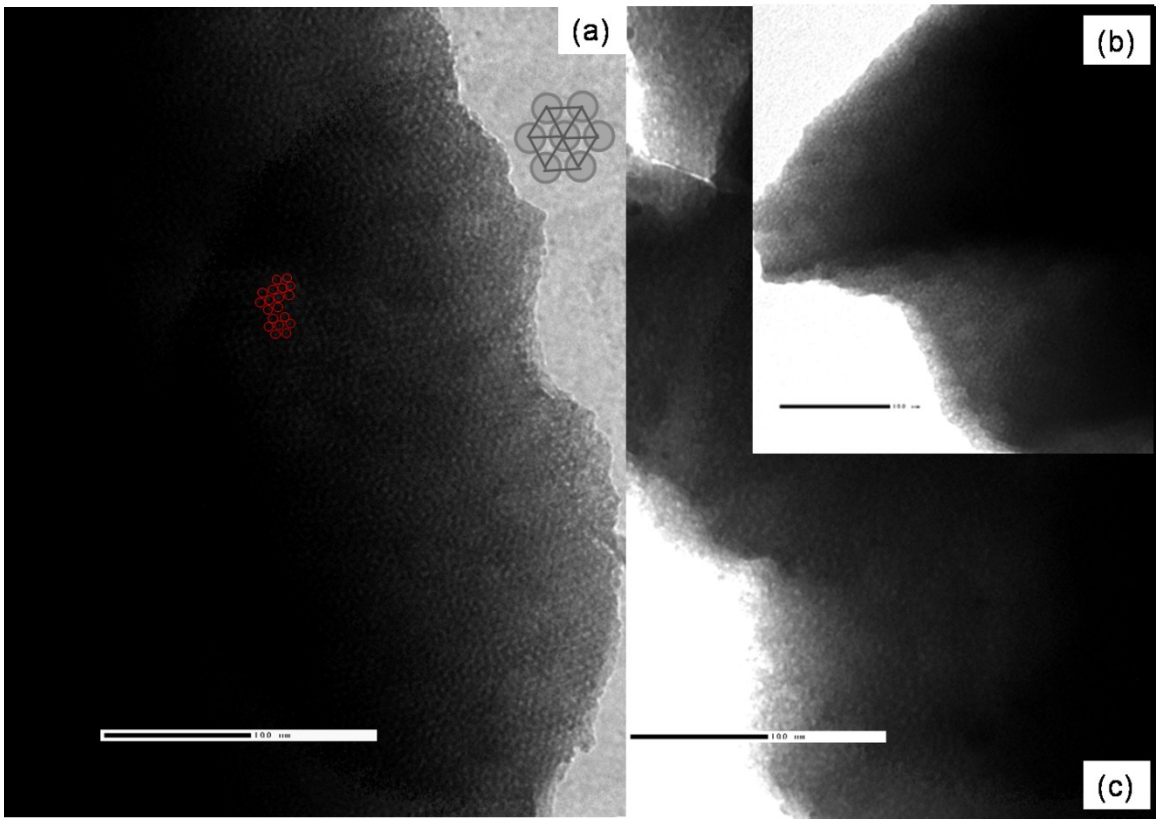

Fig. 2 TEM images of C1 TOFs in the case of single coating, heated at (a) 100 °C, 1 h, along [110] zone axe with some pores (lighter area) marked with red circles for comparison with the simulated model in the inset, in which pores are described as grey circles. (b) 250 °C, 2 h and (c) 250 °C 2 h + 400 °C, 2 h. Scale bars=100 nm.

In view of the hexagonal-like arrangement of ordered mesopores and the vertically aligned pores/channels, a cubic (bcc) mesopore structure in the mesoporous TOFs (or its rhombohedral derivative) with the [110] direction oriented is tentatively proposed. Here we rule out the possibility of a p6mm hexagonal mesoporous structure according to the above low-angle XRD results and in view of unfavorable high surface energy such

orientation might incur. No diffraction should be observed in the XRD measurement if there are no lattice planes parallel to the substrate for the sample with vertically oriented mesopore in p6mm geometry. It has been reported that Brij 56 templated silica systems also showed mesoporous structures with similar pore arrangement.[12,16] Therefore, via such a single-coating process, monomodal mesoporous TOFs can be fabricated.

This flexibility of the meso-frameworks arises from two factors: on the one hand, the EO segments in the Brij 56 molecules will be incorporated into the oxide framework walls through complexing with PTA species; on the other hand, PTA species contains significant amounts of structural water and peroxo tungsten oxide species. These moieties in the flexible PTA/Brij56 hybrid frameworks will decompose upon heat-treatment due to their lower thermal stability, leading to the shrinkage of the whole mesostructure. In view of the origin of such flexibility, it is possible to infer that, in a two-step coating process, the first coating (C1), subject to proper thermal solidification before the deposition of the second coating (C2), will experience a different heat-treatment history from C2 deposited on its top and hence result in a different mesostructure from C2. It can be expected that such difference in mesoporous structure between the two coatings might be preserved under proper conditions even after final heat-treatment at the elevated temperatures that are normally necessary to remove the organic template. Thereby the bimodal mesoporous TOFs are expected to be fabricated.

An appropriate and distinct heat-treatment step on the first coating (C1) is therefore of great importance in both solidifying C1 and bestowing C1 extra heating history compared with C2, as all the subsequent heat-treatment steps are the same for both coatings. Although heating at 100 ºC affords C1 sufficient difference in d-spacing with respect to the as-prepared mesoporous TOFs (Table 1), such heating treatment cannot solidify C1 frameworks properly. It was found that after being dried at 100 ^{o}C for 1 h, C1 still partially dissolves in the alcohol-acidic coating sol in the second dip-coating step. Theoretically, this first heat-treatment should be above the PTA's decomposition temperature, namely above 130 ^{o}C,[11] in order to solidify C1 frameworks, but below 190ºC, to prevent organic template Brij 56 from decomposition so as to avoid the interpenetration of coating sol into evacuated pore channels in the second coating step creating blockage of the pore channels of C1. Additionally, the extra heat-treatment history to C1 should be as effective as possible to render the needed mesostructural differences, which C1 will inherit and possess even after heat-treatment at high temperatures (e.g. 400 ^{o}C). In this work, it was found that heat-treatment at 170 ^{o}C for 1h meets above-mentioned requirements.

Based on this strategy, a bilayered (C1 + C2) BMM structured TOF was constructed with the C1 being heated at 170 ºC for 1h before applying the C2 coating. Fig. 1(b) shows its XRD patterns after heating at different temperatures. Compared with XRD patterns in the case of single coating, as-prepared C1 in C1+C2 shows no changes in 2θ position but a

sharp decrease in the intensity because of the shielding effect of the C2 on its top. C2 coating, on the top of C1, also shows similar resolved low-angle XRD peak (C2 peak, Fig. 1b, curve 1), indicative of the formation of comparable mesostructures on pre-deposited TOFs of C1 or on glass substrates.

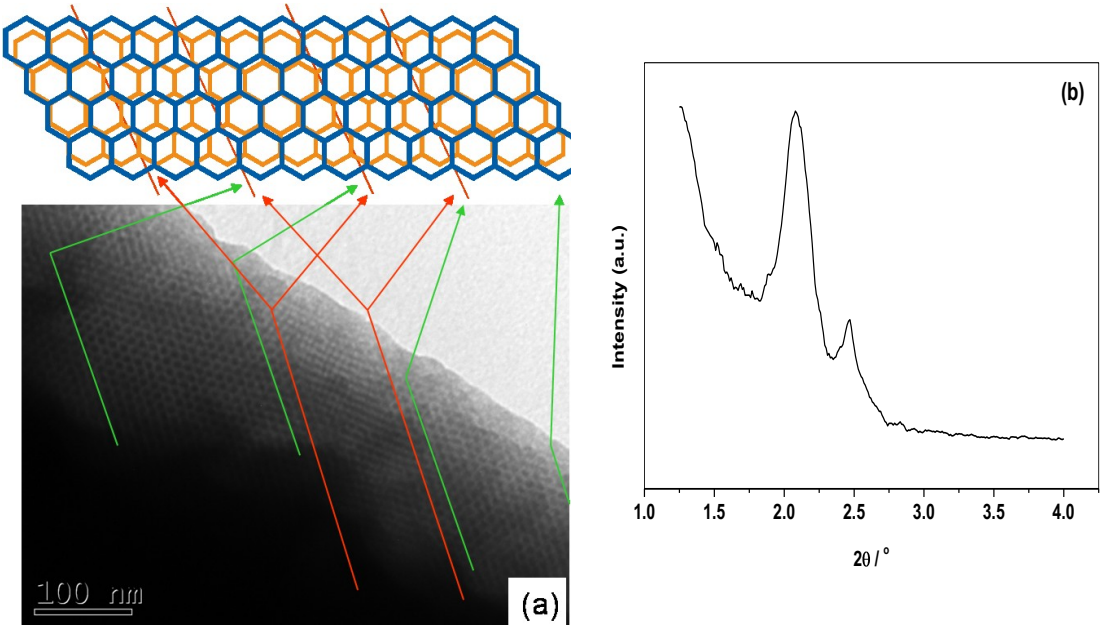

Fig. 3 (a) TEM image and (b) XRD pattern of BMM TOFs (C1+C2) heated at 100 ^{o}C for 15 h. Representative area in (a) shows the matched (between green lines) and mismatched mesopores with each other from top and bottom TOFs, which is also more clearly illustrated in the schematic model shown above the TEM image. The modelling is made according to XRD results shown in (b), with unit cell *a* values of C1 and C2 are 5.1 nm and 6.0 nm, respectively.

Fig. 3 shows the TEM image of BMM structured TOFs dried at 100 ^{o}C. We did observe the phenomena of 'interference' of BMM structures between C1 and C2 coatings in TOFs by means of TEM, thanks to the large *a* difference between C1 and C2 under such conditions. As shown in Fig. 3, regions with matched and mismatched mesopores alternate from one area to another, which is consistent with a simple modelling (See schematic shown above the TEM) using the *a* obtained from XRD results. Pore channels were also found to be open from above. As discussed above, heat treatments at high temperatures led to the formation of disordered mesostructures with diminished *a* difference. This makes it difficult to directly monitor the BMM structures by using TEM, as discussed below.

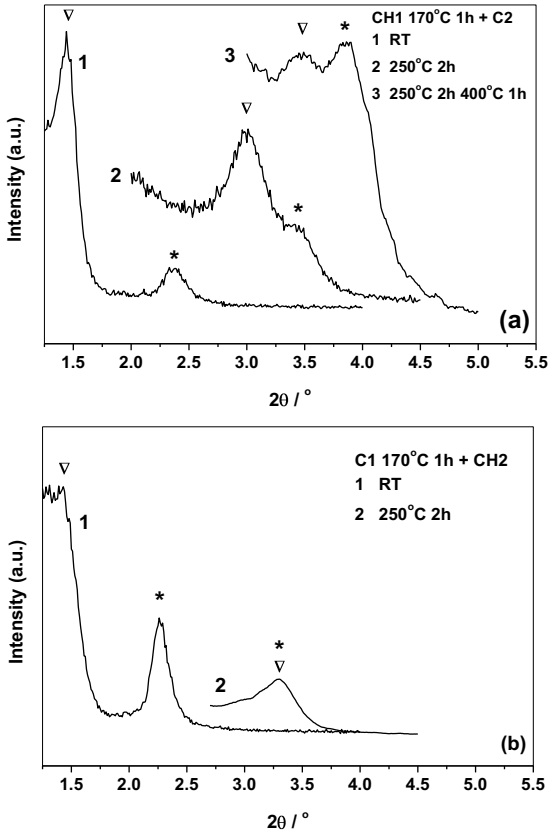

Fig. 4 XRD patterns of bimodal (a) CH1+C2 TOFs and (b) C1+CH2, heated at different temperatures with the coating 1 (bottom layer) having one more heating phase at 170 °C for 1 h. Inverted triangle represents the low-angle peak from second coating and asterisk for peak from first coating.

The double peak feature of the XRD patterns of C1+C2 bilayered BMM TOFs, was retained after heating at 250 ^{o}C for 2 h (Fig. 1(b), curve 2) being wide but with a discernable shoulder which can be de-convoluted by fitting with two Lorentzian peaks, but disappeared upon heating at 400 ^{o}C for 1h, as shown by the single peak XRD pattern (Fig. 1b, curve 3). There clearly is a tendency for re-construction of the mesostructures taking place during the heat-treatment at elevated temperatures, which is responsible for the transformation from the bimodal to mono-modal mesostructures. Actually, one trend can be observed that the low-angle XRD peaks from the C1 in single coating TOFs (2θ=3.06^{o}, 250^{o}C heated for 2 h) did not appear at the same position as C2 in the case of C1+C2 (2θ=3.11^{o}, heated for 2 h). This suggests that mesostructures of C1 and C2 are not completely independent to each other. Such direct evidence of the modification in mesostructures of the pre-deposited films (C1) by the second coating has not been observed in previous reports with bi- or multi-modal BMM structures afforded by different surfactant templates.[13a] Therefore, special measures need to be taken with an aim to reduce any such re-construction process and thus produce BMM structures even

after heat-treatment at elevated temperatures. Apparently, simply applying two coatings with different heating histories will NOT yield thermally stable BMM structures.

As discussed above, the structural water and peroxo groups in the PTA species in the PTA/Brij56 hybrid frameworks contribute to the formation of flexible mesostructures. This might provide a route to tune the hybrid frameworks' behaviour upon heat-treatment by chemically modifying the framework 'building materials'– PTA species. The tactic proposed is to make C1 more flexible by enriching the peroxo groups in the frameworks, so that it will undergo greater change upon subsequent heat-treatment. This chemical modification is implemented by adding slight higher amount of H_2O_2 to the sol (see Experimental Section). The coating derived from this modified sol is designated as CH.

Fig. 4 (a) shows the XRD patterns for TOFs with double coatings (CH1+C2) heated at different temperatures. At room temperature (Fig. 4(a), curve 1), a double peak XRD pattern is displayed, similar to that produced by the mesostructures of C1+C2 TOFs (Fig. 1(b), curve 1). The peak position of CH1 in CH1+C2 after heating at 250 ^{o}C for 2 h shifted to higher angle ($2\theta \approx 3.5^{o}$), with the d-spacing calculated to be 2.5nm in comparison with C1 in C1+C2 ($2\theta \approx 3.27^{o}$, d=2.7 nm, Fig. 1(b), curve 2, C1 peak). This supports the proposition above (i.e. the incorporation of more peroxo tungstic species makes the framework undergo greater change upon heat-treatment). As expected, the double-peak feature is retained after heating at 400 ^{o}C for 1 h (Fig. 4(a), curve 3), corresponding to a BMM structures with two d-spacings of 2.3 nm for CH1 and 2.5 nm for C2. Thus, via such two-step coating process, BMM TOFs can be successfully fabricated. It is noteworthy to note that such small difference in mesostructure dimensions between two coatings is hard to directly distinguish by means of TEM. However, considering the good consistence of XRD with TEM results as discussed above, it is safe to conclude that XRD results for BMM structured TOFs are significant. Even after heat treatment at 400 ^{o}C for 2 h, the mesoframeworks are found to be amorphous according to the wide-angle XRD results (Figure S1, Supplementary data,).

Table 2 The 2θ values and calculated unit cell sizes of C1 in C1+C2 (Fig. 1(b)) and CH1 in CH1+C2 (Fig. 3(a))

Samples	250 ^{o}C 2h		250 ^{o}C 2h+400 ^{o}C 1h	
	2θ (^{o})	a (nm)	2θ(^{o})	a (nm)
C1 in C1+C2	3.27	3.81	3.75	3.33
CH1 in CH1+C2	3.46	3.61	3.85	3.24
Difference in *a* (nm)		0.20		0.09
Difference in 2θ	0.19		0.1	

The inclusion of peroxo tungsten oxide groups inevitably modifies the wall thickness when such groups decompose upon heat-treatment.[11] One question may arise: the difference in unit cell parameter of *a* of CH1 and C2 in CH1+C2 possibly results from wall thicknesses rather than the pore size differences of these two films. Actually, the difference in films of C1 in C1+C2 (Fig. 1(b)) and CH1 in CH1+C2 (Fig. 4(a)) comes solely from the H_2O_2 modification to the latter, because the other experimental conditions are the same. It is thus possible to estimate the influence of H_2O_2 on the wall thicknesses. The 2θ values of films and calculated d-spacings were listed in Table 2. It can be seen from this table that, with the heat-treatment at 400 ^oC, the difference in 2θ values for above two films decreased by 0.1^o, with the corresponding difference in *a* being just 0.09 nm. Therefore, it can be concluded that the H_2O_2 modification has little influence on the wall thickness. In CH1+C2, the difference in unit cell size thus arises mainly from different mesopore sizes between the two layers.

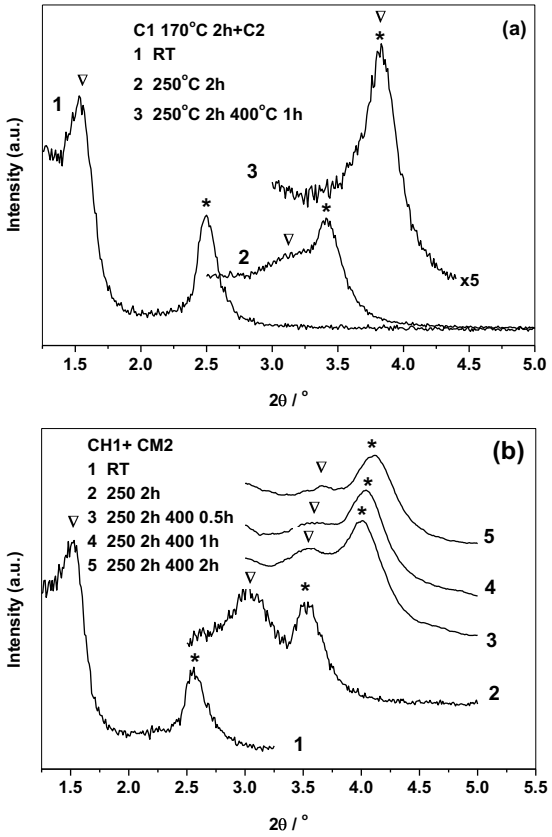

Fig. 5 XRD patterns of (a) bimodal C1 (170 ^oC 2 h)+C2 TOFs heated at different temperatures. Inverted triangle represents the low-angle peak from C2 and asterisk for peak from C1, (b) bimodal CH1+ CM2 TOFs heated at different temperatures. Inverted triangle represents the low-angle peak from CH1and asterisk for peak from CM2.

In a separate experiment, a reversed coating order, namely C1+CH2, was tested. In this case, the second coating is expected to undergo greater shrinkage upon heating. Results

shown in Fig. 4 (b) reveal that in this case BMM structures are not formed even when heat treatment is restricted to temperatures of 250 ^{o}C. It is logical that the CH2, because of more changeable mesostructures endowed by the more peroxo tungstic oxide species, is envisaged to 'catch up' the C1 during the evolution of mesostructures, even though the C1 layer has an extra heat-treatment history at 170 ^{o}C for 1 h.

In addition to using H_2O_2 to modify the inorganic frameworks, it is also possible to magnify the mesostructural difference by increasing the heating time applied on the first coating. It has been demonstrated that extending the heating time at 170 ^{o}C from 1 h to 2 h seems to be able to incur bigger structural shrinkages, as seen by shift of low-angle XRD peak to higher angles (Fig. 1(a), curves 3 and 4). Therefore, this methodology is worthy to be trialled to fabricate BMM structures. As shown in Fig. 5(a), by extending the heating time of first coating to 2 h at 170 ^{o}C, the dimension difference in mesostructures between the C1 and C2 is certainly enlarged for the as-dried C1+C2 BMM structured TOFs with the low-angle XRD peak shifted to about 2.5^{o} compared with 2.3^{o} for TOFs heated for 1h (Fig. 1(b), curve 1, C1 peak). The bimodal feature, though retained after heating at 250 °C for 2 h, disappeared after 400 °C for 1 h. Therefore, extension in heating time for first coating can further increase the initial mesostructural difference between first and second coatings, but cannot retain the difference at high temperature. This further confirms that simply applying two coatings with different heating histories without chemical modification as employed above will not yield thermally stable BMM structures.

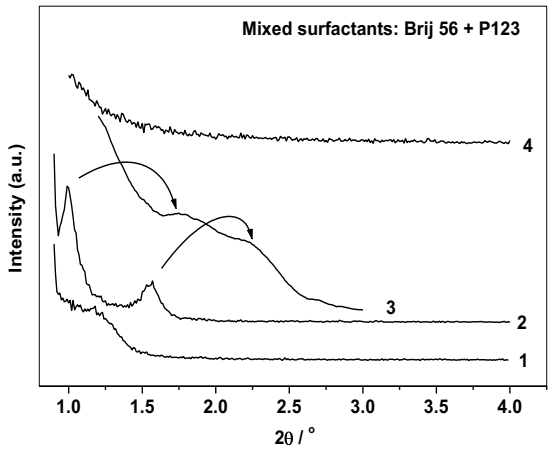

Fig. 6 XRD patterns of mixed surfactants (P123+Brij 56) templated TOFs using coating sol with (1) P123 added immediately after preparation of Brij 56 containing sol and (2-4) P123 added after aging the Brij 56 containing sol dried or heated at different temperatures: (2) room temperature, (3) 130 ^{o}C for 1 h, (4) 250 ^{o}C for 0.5 h.

Additionally, varying the solvent composition (PTA/Brij 56 species have different solubility in water and ethanol) was also investigated in order to see whether or not this factor has influence on the formation of BMM structures. Here, the formulation of the

second coating sol (denoted as CM) was changed to PTA: Surfactant: H_2O: Ethanol = 1: 0.2: 2.5: 5, hence changing the water/ethanol ratio from 2/1 to 1/2, whilst keeping the first coating (CH) unchanged. As shown in Fig. 5(b), it seems that double-peak feature for the BMM TOFs (CH1+CM2) are almost the same as that of CH1+C2 system previously shown in Fig. 4(a). Moreover, with the increasing heating time at 400 ^{o}C from 0.5 h to 2 h, the BMM structure is essentially retained, but contracts correspondingly with increasing heating time. This further proves the versatility of the technique, allowing BMM structures to be delicately tailored through simple heat-treatments at different temperatures ranging from 250 ^{o}C to 400 ^{o}C. The structural difference in *a* between the two layers after heat treatment ranges from 0.6 nm (Fig. 5(b), curve 2) to 0.3 nm (Fig. 5(b), curve 5). Such a strategy of manipulation of mesostructures by modifying the inorganic 'building materials' is quite different from methods previously reported.[3-7]

In comparison with the two-step coating process presented above, an alternative mixed surfactant templating method was also investigated to prepare BMM TOFs employing P123 and Brij 56. It has been found that the procedure of introducing P123 matters in achieving BMM TOFs. Mixing P123 with Brij 56 preceding to adding into the PTA solution [11] or addition of P123 immediately after the preparation of Brij 56-containing coating sol only led to monomodal mesoporous TOFs, as can be seen from Fig. 6 (curve 1). However, after proper aging of Brij 56-containing coating sol, addition of P123 incurred the formation of BMM TOFs (Fig. 6, curve 2 and 3). Unfortunately, all mixed surfactants (P123 + Brij 56) templated TOFs did not afford satisfactory thermal stability. Mesostructures collapsed upon heating at 250 ^{o}C, as evidenced by the disappearance of the low-angle XRD peaks (Fig. 6, curve 4). Apparently, this method of using mixed surfactant as template, though relatively more direct than two-step coating process, cannot produce thermally stable BMM TOFs. The possible reason is that in such templating system, P123 and Brij 56 cannot effectively and independently direct the formation of mesostructures in TOFs.

The electrochromic properties of obtained BMM structured TOFs (CH1+CM2) coated on ITO glasses were investigated in comparison with monomodal mesostructured TOFs (single layer CM and double layer C1+C2). The XRD patterns were shown in Fig. 7(c). As presented in Fig. 7(a), after heating at 350 ^{o}C, all the three films show good transparency indicating the essential removal of organic template. The spectra differ to some extent due to interference effects associated with the different film thicknesses. Fig. 7(b) displays their current profiles at the 8th cycle of chronoamperometry measurements in voltage steps between -0.4 V and 0.4 V (vs Ag/AgCl) (Fig. 7(b), inset). Electrochromic switching between coloration and bleaching states was clearly observed. The optical transmittance recorded at the end of the coloration and bleaching (Optical images see Fig.7a, inset) cycles together with the amounts of proton exchange associated with the electrochromic switching shown are in figure 8.

The results show that after being coloured in reduction step, CH1+CM2 TOF has much lower transmittance (≈12%) than CM, with a value of 38% transmittance being achieved in this case (at 650nm). This improved colouration can be attributed to the thickness difference of the TOFs, with thickness of the CH1+CM2 film being about 280nm, (Fig. 7(d)) compared to ~100nm for CM as measured by SEM. By comparison, Cheng, et.al,[17] reported that transmittance on mesostructured tungsten oxide films (400-500nm in thickness) was decreased to 50% transmittance under similar experimental conditions but at even lower reduction voltage (-0.8 V vs SCE (SEP is 0.24 V, which is close to that of the Ag/AgCl electrode (0.20 V) employed in this work).

Additionally, the amounts of protons inserted into CH1+CM2, namely charge density, within 30 s is about 2.2 times of those into CM, which has been reflected in their film thicknesses (Table 3). This, however, strongly supports that pore channels in CH1 film with CM2 film on top are continuous, and hence that the top coating of CM2 does not block the mesochannels of the film beneath (CH1).

The colouration efficiency (CE) that is the most relevant parameter describing the electrochromic performance of TOFs can be defined by:

$$CE = \frac{\Delta(OD)}{Q} = \frac{1}{Q} \times \log\left(\frac{T_b}{T_c}\right) = \frac{A_b - A_c}{Q} \qquad \text{(Eq.1)}$$

where, Δ(OD) is the variation in optical density, Q is the charge density (C/cm^2), T_b, T_c and A_b, A_c are the transmittance (T) and absorbance (A) in the bleached, coloured states, respectively. Based on the observation, the calculation results are shown in Table 3.

Table 3 Colouration efficiency and colouration/bleaching time of monomodal CM and BMM CH1+CM2 TOFs heated at 350 ^{o}C.

	Colouration efficiency [a] (CE)/cm^{2}C^{-1}			Coloration[b]/ Bleaching[c] time(s)	Film thickness[d] (nm)	Charge density[e] (mC/cm^2)
	1st cycle	4th cycle	8th cycle			
CM	28	49	46	11/2	100	8.2
CH1+CM2	47	44	42	11/4	280	17.5
C1+C2	48	46	44	16/4	300	23.7

a: calculated using the optical transmittance value at 650 nm. b: Time to achieve 90% of total proton insertion capacity at the 8th cycle, c: achieve 90% of total proton extraction capacity at the 8th cycle. d: estimated from SEM results (see Fig. 7(d)), e: recorded at the 8th cycle (Integration of the current density *vs* time plot shown in Fig.7(c)).

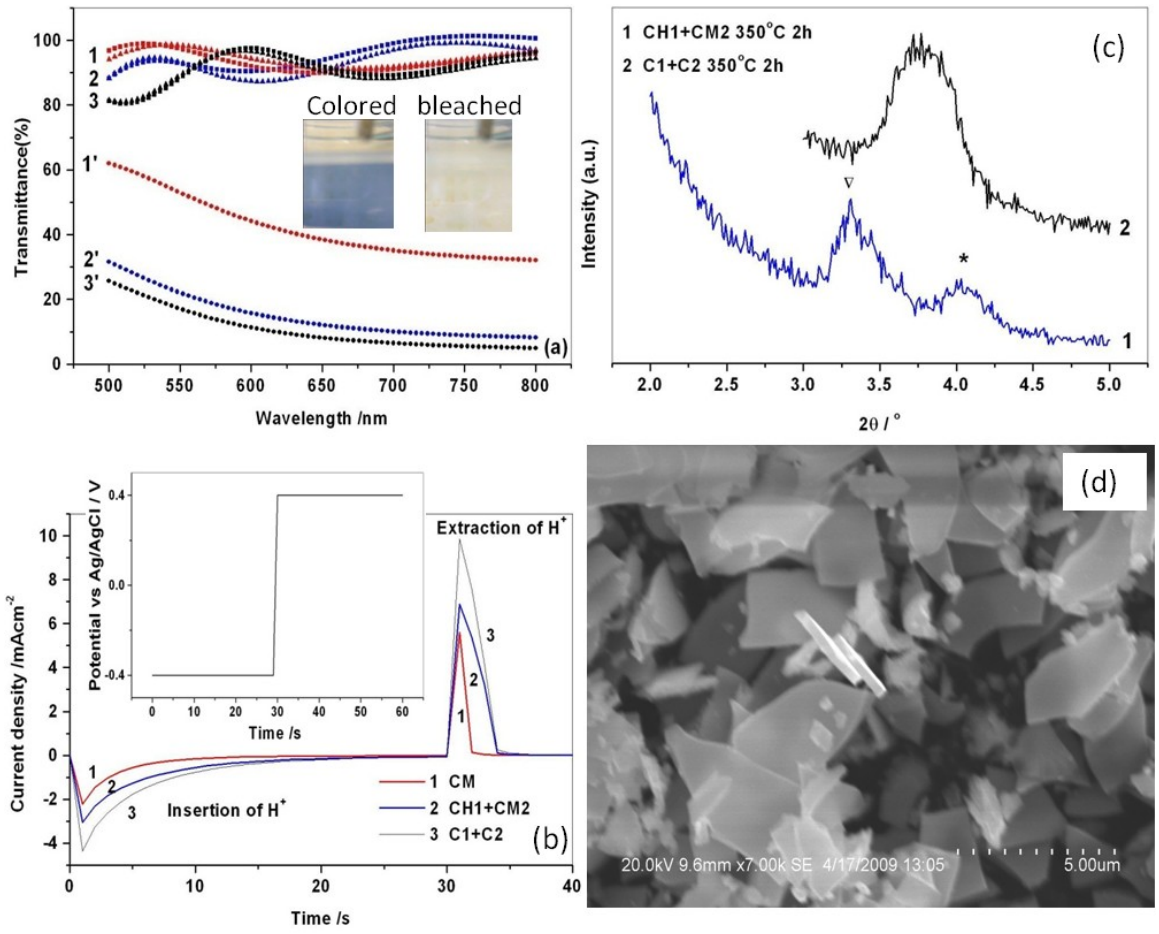

Fig.7 (a) Optical transmittance spectra for single CM TOF (curve 1 and 1′), bimodal CH1+CM2 TOF heated at 350 ^{o}C (curve 2 and 2′) and monomodal C1+C2 TOF (curve 3 and 3′). Numbers without apostrophes (e.g. 1, 2 and 3) and those with apostrophe (e.g. 1', 2' and 3') denote samples in bleached/original states and coloured states (8th cycle, see inset), respectively. Curve 1 or 2 or 3 each is composed of two curves, one of which denotes the bleached state and the other is for original states. Because optical transmittance spectra for original state and bleached state are quite close to each other, they are denoted together by just one number for simplicity. (b) Chronoamperometry measurements (8th cycle) in voltage steps between -0.4 V and 0.4 V (vs Ag/AgCl) (shown inset) of samples: (1) CM TOF, (2) bimodal CH1+CM2 TOF and (3) monomodal C1+C2 TOF. (c) Low-angle XRD patterns of (1) bimodal CH1+CM2 and (2) monomodal C1+C2 TOFs. Inverted triangle represents the low-angle peak from CM2 and asterisk for peak from CH1. (d) SEM micrograph of bimodal TOFs of CH1+CM2.

The comparable CE values for both CM (46 cm^{2}C^{-1}) and CH1+CM2 (42 cm^{2}C^{-1}) reported in this work are much higher than the values reported on other mesoporous TOFs (23.5 cm^{2}C^{-1} for 300 ^{o}C heated film and 35.8 cm^{2}C^{-1} for 400 ^{o}C heated film) reported in ref [17] and approach the top of the typical range (30-50 cm^{2}C^{-1}) of values reported for conventional tungsten oxide films [18]. Compared with CE values at 4th and 8th cycles, the much lower CE value at 1st cycle for CM can be attributed to the higher amount of

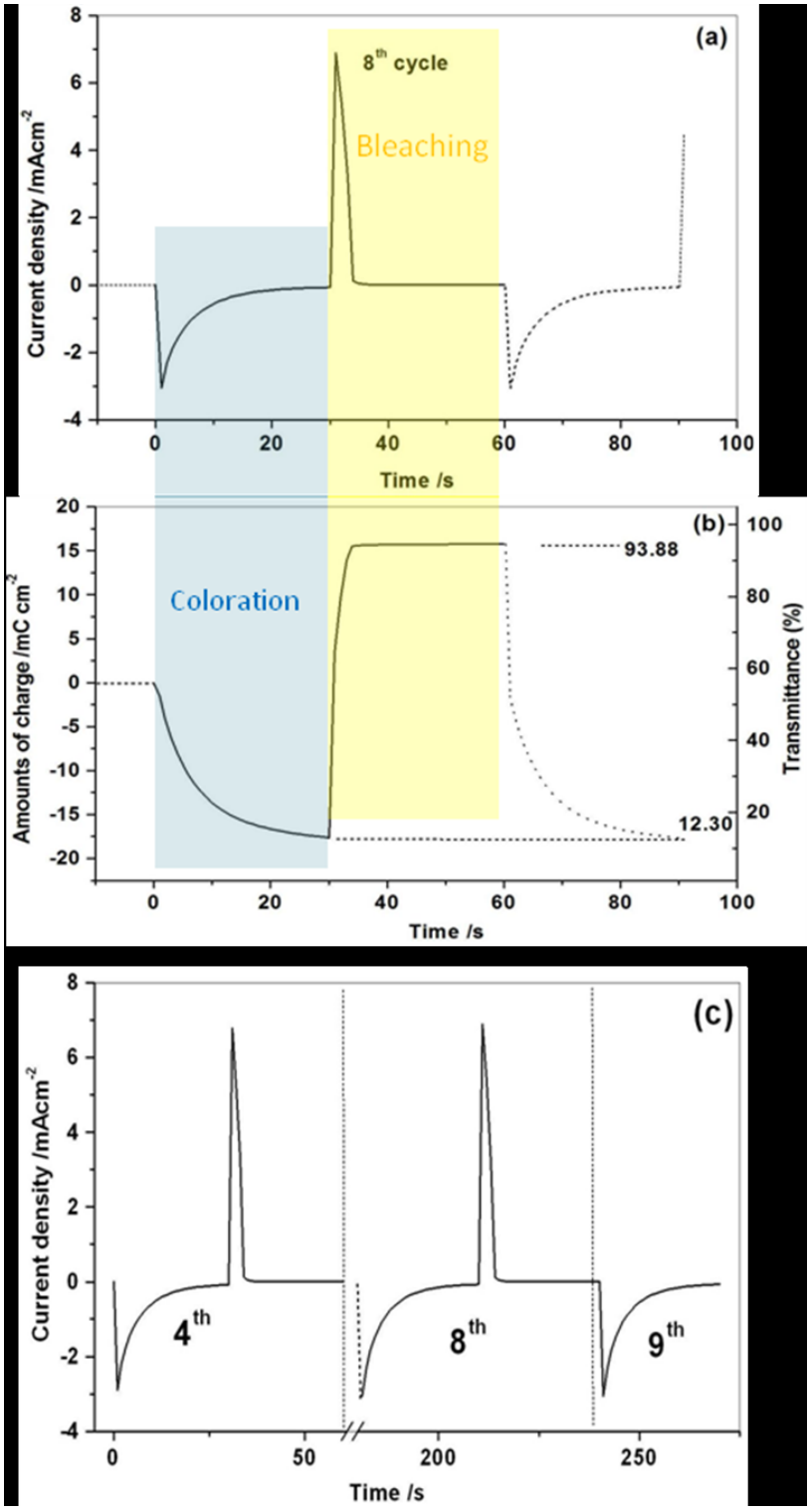

Figure 8(a) Chronoamperometry measurements (8th cycle) in voltage steps between -0.4 V and 0.4 V (vs Ag/AgCl) of bimodal CH1+CM2 TOF, (b) integrated amounts of charge and recorded transmittance at 650 nm at the end of reductive and oxidative cycles. Measurement was performed at voltage steps between -0.4 V and 0.4 V (vs Ag/AgCl) .(c) Comparison between different cycles.

protons (Q) inserted during the 1st colouration, in which all kinds of accessible injection sites are occupied, including those irreversible ones (some charges counted at this cycle will not be recordable at later cycles). In addition, the lower thickness of CM might also be responsible for different chemical diffusion behaviour in comparison to the other thick films (e.g. CH1+CM and C1+C2). The effect of a lower CE value during the first cycle was also observed in other studies on mesoporous TOFs by Cheng, et al [17].

The CH1+CM2, although, showing slightly inferior bleaching speed (<4 s) to CM (2s, see Fig. 7(b) and Table 3), is demonstrated to be comparable or better than lamellar phase mesoporous tungsten oxide tested under similar conditions, [19] in which bleaching time of 5 s needed to be taken to extract majority of the inserted protons. It has also shown to be superior over P123 surfactant templated tungsten oxide film (heated at 400°C, in which coloration time (40% transmission) and bleaching time were recorded for 26s and >30s, respectively [17]). Such exciting electrochromic properties shown by CH1+CM2 are believed to result from well-preserved BMM structures. Some of these characteristics show some improvement in the when compared with other non-mesoporous TOFs with very fast responses [20]. However, in comparison with these electrochemically grown and etched WO_3 films[20] the response times of the materials developed here are somewhat slower. However, interestingly this does offer the prospect of further enhancements if the etching technique developed for these electrochemically grown films could be applied to these new materials.

Upon the insertion and extraction of protons, the colors of BMM TOFs switched between blue (colored state) and transparent, as tinted by light blue and yellowish, respectively. The recorded transmittance changes accordingly. The transmittances at 650nm recorded at the end of coloration and bleaching were read and marked on the figure 8(b). The EC switching behaviours at different cycles (4, 8 and half 9th) are quite consistent, as can be seen from 8(c).

Importantly, BMM structured CH1+CM2 did show shorter response time than monomodal mesostructured C1+C2 (Table 3). The probable reason is due to the wider opening mesostructure (about 0.4nm in *a*, Fig. 7(c)) of the CM2 in CH1+CM2 than C2 in C1+C2, which facilitate the protons diffusion from the bulk electrolyte solution to the WO_3 surface. Bimodal TOFs developed in this work showed balanced electrochromic properties in terms of coloration efficiency, response times and transmission modulation capability, and is thus deemed to be superior over their monomodal mesostructured counterparts in electrochromic applications.

As peroxo species, e.g. H_2O_2, is a common complexing agent for many transition metal (V, Ti, Mo, Nb, etc.) ions, it is proposed that such strategy brought up in this work would therefore open a new way to prepare a range of transition metal oxides with controlled, delicate bimodal mesostructures, which could find applications, e.g. in catalysis.

Extended works are undergoing to investigate the applicability of such synthesis strategy for other transition metal oxide systems.

3. Experimental

Materials: Tungstic acid (≥99.0%) was obtained from Fluka, H_2O_2 35wt.% water solution and the non-ionic surfactant Brij56 ($C_{16}EO_{10}$, $C_{16}H_{33}(OCH_2CH_2)_nOH$, n~10), P123 ($H(OCH_2CH_2)_{20}(OCH(CH_3)CH_2)_{70}(OCH_2CH_2)_{20}OH$), were purchased from Aldrich. All the chemicals were used as received.

Sol-gel meso-films: The coating sols were prepared according to previous report with some modifications [11]. The tungstic acid was converted to peroxotungstic acid (PTA) in water. Obtained PTA powders were collected after drying at 40 ^oC for later use. The coating sol was prepared as mixed solution of PTA, Brij56 in water and ethanol, with a final weight ratio of PTA: Surfactant: H_2O: Ethanol of 1: 0.2: 4.5: 2.25. An additional small amount of H_2O_2 (in weight ratio of about 1:80 to the prepared sol) may be duly added to modify the sol. Obtained sols were used for dip-coating on cleaned glass substrates under ambient conditions or in the case of samples used for testing electrochromic properties, indium-tin oxide (ITO) coated glass substrates. The deposited films were allowed to dry at room temperature and then, further thermally treated at temperatures of 100-400 ^oC to solidify the film and remove the template as appropriate. The coatings deposited using H_2O_2 modified and unmodified coating sols were designated as 'CH' and 'C', respectively, with the following numbers, e.g. 1 or 2, which represent the first or the second coating. For example, CH1 means the first coating deposited on substrate using H_2O_2 modified sol.

Mixed surfactants templated sol-gel films: For the samples using mixed surfactant templates, the coating and following drying and heating processes are the same, except that for the Brij56-containing coating sol, after aging properly, a small amount of P123 dissolved in the mixture of water and ethanol (2:3, w/w) was added.

Characterisation: XRD measurement was conducted on Siemens D500/D501 with CuK_α radiation (λ=0.1542 nm) at a scanning speed of 0.01^o per second, using low angle diffraction peaks to determine the d-spacings according to the normal Bragg relationship. Low angle X-ray diffraction (XRD) provides a broad view of mesostructures of the sample. In this work, the position of the diffraction peaks is reported as a proxy for the mesoporosity dimension. Accurate estimation of the pore spacing requires the mesostructures to be highly ordered with known geometry. In similar Brij 56 templated silica system, cubic mesoporous structures was reported [12,16]. The unit cell parameter (a) for the cubic mesostructure is calculated from d(110) according to $a = d_{hkl}\sqrt{h^2+k^2+l^2}$, where d(110) is obtained from the 2θ value of the main peak in the XRD pattern from $d(110)=\lambda/2\sin(\theta)$, where λ = 0.15417 nm for the Cu Kα line. Transmission electron

microscopy analysis was performed at different magnifications using JEOL 2100FX TEM. Samples for TEM measurement were obtained by scratching off coated films from the glass substrates, and this being dispersed in acetone and mounted on copper grids. SEM images were recorded using S3400N Scanning Electron Microscope.

Electrochromic property measurement: The electrochemical properties were determined using a three electrode configuration in which the working electrode consisted of the dip coated TOFs deposited on ITO coated glass in 0.1 M aqueous solution of sulphuric acid. An Ag electrode (Ag|AgCl|saturated KCl) and a platinum needle were taken as the reference and counter electrode, respectively. The experiments were performed using an Autolab 12 potentiostat with GPES software for collection and analysis of data. The optical spectra were collected using a Jasco V-630/630BIO UV-Vis spectrophotometer with scanning speed of 200 nm/min.

4. Conclusions

A novel two-step coating process to engineer mesostructures through modifying the inorganic frameworks was successful developed and employed to fabricate bimodal meso-mesoporous tungsten oxide films. Specifically, chemical modification using H_2O_2 to enrich the peroxo tungsten oxide species in the PTA/Brij56 hybrid frameworks imparted both more flexibility, and more thermal sensitivity (shrinkage) than its unmodified counterpart, and was demonstrated to be successful in promoting the preservation of BMM structures of TOFs upon heat-treatment at elevated temperatures (e.g. 400 ^{o}C). By application of two coatings differently thermally sensitised by the addition of H_2O_2, differential structural changes on heat treatment can be used to engineer a bimodal meso-mesoporous structure. The mesostructural difference in *a* between these layers can be tailored in the range of 0.2-0.6 nm by heat treatments under different conditions.

Such bimodal mesostructured TOFs showed much improved electrochromic properties compared with those been reported by other research groups,[17,19] in terms of colouration effects, with transmittance decreased from over 90% to 16% at -0.4 V(vs Ag) in 30 s, and greatly enhanced coloration efficiency of up to 42cm^{2}C^{-1}. Additionally, BMM TOFs developed in this work showed balanced electrochromic properties and are thus believed to be superior over their monomodal mesostructured counterparts from the viewpoint of application.

Acknowledgement

The DTI support (TP-CHBT-006-00015) for this work under the project "Sol-Gel nanocoatings for design & development of new generation subminiature fluorescence lamps" is gratefully acknowledged. Special thanks to Mr. John Bates for his kind help in TEM measurements in the Loughborough Materials Characterization Center (LMCC) at

Loughborough University, Loughborough, UK.

References:

1 (a) C. T. Kresge, M. E. Leonowicz, W. J. Roth, J. C. Vartuli, J. S. Beck, *Nature*, 1992, **359**, 710-712. (b) J. S. Beck, J. C. Vartuli, W. J. Roth, M.E. Leonowicz, C. T. Kresge, K. D. Schmitt, C. T.-W. Chu, D. H. Olson, E. W. Sheppard, S. B. McCullen, J. B. Higgins, J. L. Schlenkert, *J. Am. Chem. Soc.,* 1992, **114**, 10834-10843.

2 (a) C. G. Goltner, M. Antonietti, *Adv. Mater.,* 1997, **9**, 431-436. (b) A. Stein, B. J. Melde, R. C. Schroden, *Adv. Mater.,* 2000, **12**, 1403-1419.(c) G. J. A. A. Soler-Illia, C. Sanchez, B. Lebeau, J. Patarin, *Chem. Rev.,* 2002**, 102**, 4093-4138.(d) C. Sanchez, C. Boissière, D. Grosso, C. Laberty, L. Nicole, *Chem. Mater.,* 2008, **20**, 682-737. (e) S. Pokhrel , C. E. Simion , V. S. Teodorescu , N. Barsan , U. Weimar, *Adv. Funct. Mater.,* 2009, **19**, 1767-1774.

3 (a) H. Mori, M. Uota, D. Fujikawa, T. Yoshimura, T. Kuwahara, G. Sakai, T. Kijima, *Micropor. Mesopor. Mater.*, 2006, **91**, 172-180. (b) T. Brezesinski,C. Erpen, K. Iimura, B. Smarsly, *Chem. Mater.,* 2005, **17**, 1683-1690.

4 K. Nakanishi, R. Takahashi, T. Nagakane, K. Kitayama, N. Koheiya, H. Shikata, N. Soga, *J. Sol–Gel Sci. Technol.,* 2000, **17**, 191-210.

5 (a)F. Q. Zhang, Y. Yan, Y. Meng, Y. Xia, B. Tu, D. Y. Zhao, *Micropor. Mesopor. Mater.,* 2007, **98***,* 6-15. (b) L. Xiong, J. Shi, L. Zhang, M. Nogami, *J. Am. Chem. Soc.,* 2007, **129**, 11878-11879. (c) Q. Xiao, Y. Zhong, W. Zhu, T. Chen, L.Wang, *Micropor. Mesopor. Mater.,* 2008, **116**, 339-343. (d) M. Tortajada, D. Ramón, D. Beltrán, P. Amorós, *J. Mater. Chem.*, 2005, **15**, 3859–3868. (e) K. Suzuki, A. K. Sinha, *J. Mater. Chem.,* 2007, **17**, 2547–2551.

6 (a)J. Sun, Z. Shan, T. Maschmeyer, J.A. Moulijn, M.O. Coppens, Chem. Commun., 2001, 2670-2671. (b) J. Sun, Z. Shan, T. Maschmeyer, M. Coppens, *Langmuir*, 2003, **19**, 8395-8402.

7 Z. Y. Yuan, J. L. Blin, B. L. Su, *Chem. Commun.,* 2002, 504.

8 F. Schüth, *Chem. Mater.,* 2001, **13**, 3184-3195.

9 P. M. S. Monk, R. J. Mortimer D. R. Rosseinsky, Electrochromism and Electrochromic Devices, Cambridge University Press, Cambridge. 2007.

10 (a) M. Deepa, A. K. Srivastava, K. N. Sood, S. A. Agnihotrym, *Nanotechnology,* 2006, **17**, 2625-2630. (b) M. Deepa, A. K. Srivastava, S. N. Sharma, Govind, S. M. Shivaprasad, *Appl. Surf. Sci.,* 2008, **254**, 2342-2352.

11 W. Wang, Y. X. Pang, S. N. B. Hodgson, *Micropor. Mesopor. Mater.,* 2009, **121**,121-128.

12 C. J. Brinker, Y. Lu, A. Sellinger, H. Fan, *Ad*v. *Mater.,*1999, **11**, 579-585.

13 (a) P. C. Angelomé, M. C. Fuertes, G. J. A. A. Soler-Illia, *Adv. Mater.,* 2006, **18**, 2397-2402. (b) M. C. Fuertes, F. J. López-Alcaraz, M. C. Marchi, H. E. Troiani, V. Luca, H. Míguez, G. J. A. A. Soler-Illia, *Adv. Funct. Mater.,* 2007, **17**, 1247-1252.

14 J. Y. Ying, C. P. Mehnert, M. S. Wong, *Angew. Chem. Int. Ed.*, 1999, **38**, 56-77.

15 H. Choi, A. C. Sofranko, D. D. Dionysiou, *Adv. Funct. Mater.,* 2006, **16**, 1067-1074.

16 A. P. Singh, D. D. Gandhi, B. Singh, E. Simonyi, E. G. Liniger, S. V. Nitta,M. W. Lane, G. Ramanath, *Appl. Phys. Lett.,* 2009, **94**, 093502-1-093502-3.

17 W. Cheng, E. Baudrin, B. Dunn, J. I. Zink, *J. Mater. Chem.,* 2001, **11**, 92-97.

18 C. G. Granqvist, Handbook of Inorganic Electrochromic Materials, Elsevier, Amsterdam, 2002.

19 S. H. Baeck, K. S. Choi, T. F. Jaramillo, G. D. Stucky, E. W. McFarland, *Adv. Mater.,* 2003, **15**, 1269-1273.

20 (a) M. Hepel, H. Redmond, I. Dela, *Electrochim. Acta*, 2007, **52**, 3541–3549. (b)M. Hepel, H. Redmond, *Cent. Eur. J. Chem.*, 2009 ,**7**, 234-245.